

Scene Splatter: Momentum 3D Scene Generation from Single Image with Video Diffusion Model

Shengjun Zhang¹, Jinzhao Li¹, Xin Fei¹, Hao Liu², Yueqi Duan^{1†}

¹Tsinghua University, ²WeChat Vision, Tencent Inc.

{zhangsj23, lijinzha22}@mails.tsinghua.edu.cn, duanyueqi@tsinghua.edu.cn

<https://shengjun-zhang.github.io/SceneSplatter/>

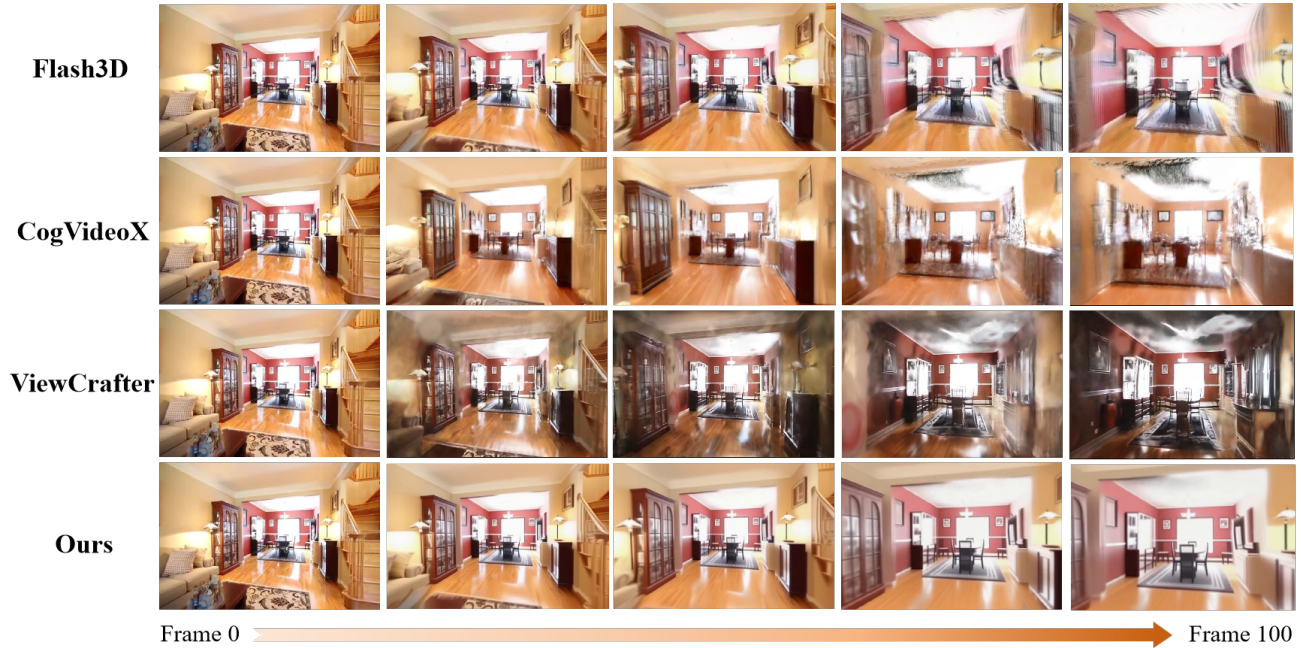


Figure 1. Visualization results of Flash3D [31], CogVideoX [42], ViewCrafter [45] and ours. Flash3D [31] suffers from distortions and occlusions, while CogVideoX [42] and ViewCrafter [45] change the color style or existing components, compared to the input image. Our method can generate high fidelity and consistent 3D scene with our cascaded momentum.

Abstract

In this paper, we propose *Scene Splatter*, a momentum-based paradigm for video diffusion to generate generic scenes from single image. Existing methods, which employ video generation models to synthesize novel views, suffer from limited video length and scene inconsistency, leading to artifacts and distortions during further reconstruction. To address this issue, we construct noisy samples from original features as momentum to enhance video details and maintain scene consistency. However, for latent features with the perception field that spans both known and unknown regions, such latent-level momentum restricts

the generative ability of video diffusion in unknown regions. Therefore, we further introduce the aforementioned consistent video as a pixel-level momentum to a directly generated video without momentum for better recovery of unseen regions. Our cascaded momentum enables video diffusion models to generate both high-fidelity and consistent novel views. We further finetune the global Gaussian representations with enhanced frames and render new frames for momentum update in the next step. In this manner, we can iteratively recover a 3D scene, avoiding the limitation of video length. Extensive experiments demonstrate the generalization capability and superior performance of our method in high-fidelity and consistent scene generation.

[†]Corresponding author.

1. Introduction

Recovering 3D models from 2D images is a fundamental problem in computer vision, due to its widespread applications, such as virtual reality, augmented reality, robotics and so on. Recently, 3D neural reconstruction techniques, such as NeRF [22] and 3D Gaussian Splatting (3DGS) [12] has achieved remarkable progress. Despite of their high quality in dense view reconstruction, generating a scene from one single view is still an ill-posed problem, since unambiguous geometric cues and occluded parts are unavailable in the monocular setting.

Previous methods attempt to learn scene prior knowledge from additional training data with various techniques, such as ResNet [31, 43], epipolar transformer [2] and cost volume [3, 5], to synthesize novel views from sparse or single input. However, these methods struggle to acquire high-quality renderings in unseen areas, especially with out-of-distribution input data. As shown in Figure 1, Flash3D [31] fails to recover unknown regions and suffers from distortions in geometry. Recent advancements in powerful generative models have promoted 3D generation from single input. Some methods [14, 15, 18, 28] generate multi-view images for reconstruction, but they are restricted to object-level generation. Other methods [8, 13, 29] apply 2D diffusion models for per-view inpainting. Yet, they often generate inconsistent contents with semantic drifts.

We analogy novel view synthesis to the generation of continuous video frames, and reformulate the challenging 3D consistency problem as temporal consistency within video generation, to unleash the strong generative prior of pre-trained large video diffusion models [19, 45]. An intuitive idea is to directly recover 3D scene from generated videos. As illustrated in Figure 1, we adopt CogVideoX [42] and ViewCrafter [45] to enhance the view synthesis process, but they change the property of existing components, leading to conflicts in 3D reconstruction. To address these issues, we propose Scene Splatter, a momentum 3D scene generation paradigm to introduce existing scene information as momentum in the generation process, to balance the generative prior and scene consistency. Specifically, we construct noisy samples from original features as latent-level momentum to guide each denoising step, avoiding the change of existing components in multiple steps of reverse diffusion. For latent features covering both known and unknown regions, latent-level momentum restricts the generation of unseen regions. Therefore, we decode the denoised latent features to RGB space and inject this consistent video as pixel-level momentum to a generated video without aforementioned latent-level momentum for further enhancement of unknown areas. We finetune the global Gaussian representations supervised by the enhanced views. Instead of high-level camera pose prompts [9, 39], we follow our predefined camera trajectory to obtain ren-

dering results from Gaussian representations for momentum update in the next generation step. In this manner, we can iteratively recover a 3D model from one single image, avoiding the inherent restriction of video length in diffusion models.

Experimental results show that our method outperforms regression-based and generation-based baselines for high quality and scene consistency, unveiling the immense potential to create complex 3D scenes using video diffusion models. Our contributions can be summarized as follows:

1. We introduce Scene Splatter, a momentum based framework that generates 3D scenes from one single image while maintaining high quality and scene consistency.
2. We construct latent-level and pixel-level momentum from Gaussian representations for generation process to balance generative prior and existing scene information.
3. Qualitative and quantitative results demonstrate that our method achieve superior performance with high-fidelity and generalizability.

2. Related Works

2.1. Regression Model for 3D Reconstruction

Recent advancements in neural representations have promoted the development of 3D reconstruction. Neural Radiance Field [22] and 3D Gaussian Splatting [12] require dense input views for per-scene optimization, and suffer from overfitting with few inputs. Early attempts [3, 7, 25, 34, 43] on NeRF opt for pretraining on extensive datasets to impart prior knowledge. Similar ideas [2, 5, 31, 32, 36, 47] are adopted to 3DGS, to predict scene-level Gaussian representations. For sparse view inputs, pixelSplat [2] applies an epipolar transformer to extract scene features from image pairs, while MVsplat [5] constructs cost volume representation via plane sweeping to produce 3D Gaussians in a faster way. For single view inputs, Flash3D [31] adopts a pre-trained depth network and predict multi-layer Gaussians. However, they are limited by the scarcity and diversity of 3D data and struggle to acquire accurate geometric cues in unseen areas for high-quality renderings .

2.2. Generative Model for 3D Reconstruction

The rapid development in 2D diffusion models [11, 26, 30] have shown exceptional generative capability, which can be leveraged for 3D Generation. Previous studies distill the knowledge in the pre-trained 2D diffusion models [24, 27] into a coherent 3D model with the Score Distillation Sampling technique [16, 38, 40]. To enhance the 3D consistency, several works [17, 18, 20, 33] have conditioned 2D diffusion models on multi-view camera poses. For example, Wonder3D [20] employs a multi-view cross-domain attention mechanism to exchange information across views and modalities. Yet, these methods are restricted to object-level

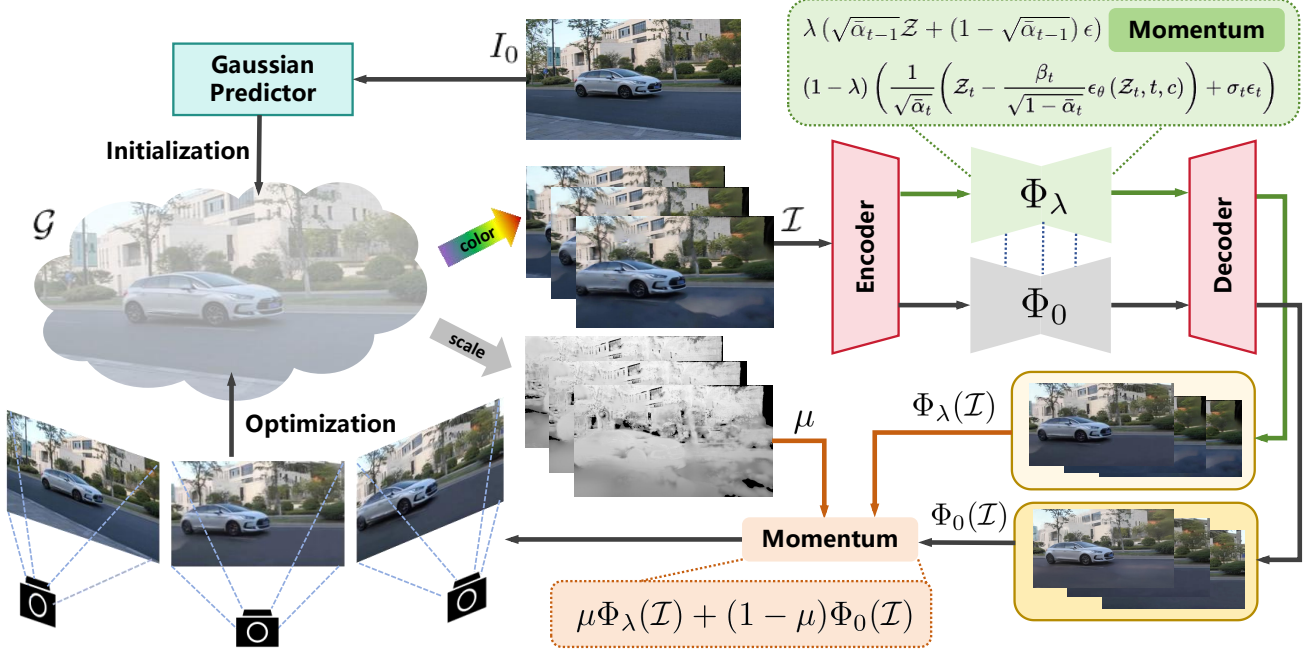


Figure 2. The pipeline of Scene Splatter. We initialize the Gaussian representations from the input image I_0 with a Gaussian Predictor [31]. For each iteration, we first render the video \mathcal{I} from 3D Gaussians \mathcal{G} . Then, we generate the enhanced video $\Phi_\lambda(\mathcal{I})$ with latent-level momentum and $\Phi_0(\mathcal{I})$ directly from the vanilla diffusion model, where Φ_λ and Φ_0 share the same weights of the denoising network. We further render scale maps as pixel-level momentum coefficient to further enhance the generated frames. We use the final results to supervise the optimization of Gaussian representations. We conduct this process along the camera trajectory to iteratively recover 3D scenes.

generation. Some other researches [29, 44] follow the iterative processes of unprojecting, rendering and outpainting to synthesize novel views from a single image. Nevertheless, they often suffer from inconsistent generated contents and semantic drifts. More recently, video diffusion models [1, 4, 10, 41] have shown an impressive ability to produce realistic videos for 3D generation [6, 35]. However, some methods [42, 45] change the property of existing components when enhancing input videos, while other methods [9, 39] lack precise control of the camera motion due to their explicit injection of high-level camera pose prompts to video diffusion models.

3. Methods

The pipeline of our framework is illustrated in Figure 2. In Section 3.1, we briefly review 3D Gaussian Splatting and video diffusion models. In Section 3.2, we propose our latent-level and pixel-level momentum for scene generation. In Section 3.3, we introduce details of the overall architecture to recovery 3D scenes from single inputs.

3.1. Preliminary

3D Gaussian Splatting. 3DGS [12] represents a scene as a set of 3D Gaussian primitives, including a center position $\mu \in \mathbb{R}^3$, a covariance matrix $\Sigma \in \mathbb{R}^{3 \times 3}$, an opacity

$\alpha \in [0, 1]$ and spherical harmonics coefficient $c \in \mathbb{R}^k$. The Gaussian function can be formulated as:

$$G(x) = e^{-\frac{1}{2}(x-\mu)^\top \Sigma^{-1}(x-\mu)}, \quad (1)$$

where $\Sigma = RSS^\top R^\top$, S is the scaling matrix and R is the rotation matrix. For every pixel, the color is rendered by a set of Gaussians sorted in depth order:

$$C = \sum_{i \in N} c_i \alpha_i \prod_{j=1}^{i-1} (1 - \alpha_j). \quad (2)$$

Video Diffusion Models. Diffusion models have emerged as the dominant paradigm for video generation, including two primary components. The forward process gradually transform a clean data sample $x_0 \sim p(x)$ to a Gaussian noise $x_T \sim \mathcal{N}(0, I)$ by

$$x_t = \sqrt{\bar{\alpha}_t} x_0 + \sqrt{1 - \bar{\alpha}_t} \epsilon, \epsilon \sim \mathcal{N}(0, I) \quad (3)$$

where x_t and $\bar{\alpha}_t$ denotes the noisy data and noise strength at the timestep t . The reverse process removes noise from the clean data by predicting the noises:

$$x_{t-1} = \frac{1}{\sqrt{\bar{\alpha}_t}} \left(x_t - \frac{\beta_t}{\sqrt{1 - \bar{\alpha}_t}} \epsilon_\theta(x_t, t, c) \right) + \sigma_t \epsilon_t, \quad (4)$$



Figure 3. Visualization of vanilla video diffusion model [45] and our two level momentum. We observe that latent-level momentum can enhance details (red box) while maintaining consistency (blue box). Yet, such momentum limits the generation ability for unseen regions (green box). Motivated by this observation, we further propose pixel-level momentum to benefit from both (c) and (d).

where c represents the embeddings of conditions, ϵ_θ is the denoising network and $\epsilon_t \sim \mathcal{N}(0, I)$. The optimization objective is defined as

$$\mathcal{L} = \mathbb{E}_{\epsilon \sim \mathcal{N}(0, I), t} [\|\epsilon - \epsilon_\theta(x_t, t)\|_2^2], \quad (5)$$

For video generation, latent diffusion models [26] are commonly employed to mitigate the computational cost.

3.2. Momentum Scene Generation

Given the global Gaussian representations \mathcal{G} and the target camera trajectory $\mathcal{K} = \{K_i\}_{i=1}^N$, we can render a video:

$$\mathcal{I} = \{I_i\}_{i=1}^N = \psi_c(\mathcal{G}, \mathcal{K}), \quad (6)$$

where I_i is the rendering image corresponding to viewpoint K_i . To enhance the quality of novel view rendering, we leverage latent video diffusion models (VDM) [1, 41, 42] trained on large-scale video datasets. VDMs consist of a pair of VAE encoder \mathcal{E} and decoder \mathcal{D} to transfer videos between the RGB space and the latent space, and a video denoising network to remove noises on noisy latents.

Latent-level Momentum. We encode \mathcal{I} and the input image I_0 to latent space:

$$\mathcal{Z} = \{Z_i\}_{i=1}^N = \mathcal{E}(\mathcal{I}), \quad Z_0 = \mathcal{E}(I_0), \quad (7)$$

where $Z_i \in \mathbb{R}^{hw \times C}$ is the latent feature of I_i . We introduce noisy samples directly from \mathcal{Z} as our latent-level momentum. Then, the reverse process in Eq. 4 can be reformulated as:

$$\begin{aligned} Z_{t-1} &= \lambda(\sqrt{\alpha_{t-1}}Z + (1 - \sqrt{\alpha_{t-1}})\epsilon) \\ &+ (1 - \lambda) \left(\frac{1}{\sqrt{\alpha_t}} \left(Z_t - \frac{\beta_t}{\sqrt{1 - \alpha_t}} \epsilon_\theta(Z_t, t, c) \right) + \sigma_t \epsilon_t \right), \end{aligned} \quad (8)$$

where $\epsilon \sim \mathcal{N}(0, I)$ is a random noise and λ is the momentum coefficient. Instead of treating λ as a hyperparameter [21], we design the following strategy to compute the momentum coefficient $\lambda = \{\lambda_i^j\}_{\substack{1 \leq j \leq hw \\ 1 \leq i \leq N}} \in \mathbb{R}^{N \times hw}$. We hypothesize the first n frames of \mathcal{I} are well-generated, and construct a latent pool from Eq. 7:

$$\mathcal{Z}_{ref} = \{Z_0\} \cup \{Z_i\}_{i=1}^n \in \mathbb{R}^{(n+1)hw \times C}. \quad (9)$$

Algorithm 1 latent-level Momentum

Input: The reference image I_0 , camera parameters $\mathcal{K} = \{K_i\}_{i=1}^N$ and Gaussian representations \mathcal{G}

Output: Enhanced frames $\tilde{\mathcal{I}}$

$$\mathcal{I} = \{I_i\}_{i=1}^N = \psi_c(\mathcal{G}, \mathcal{K})$$

$$\mathcal{Z} = \{Z_i\}_{i=1}^N = \mathcal{E}(\mathcal{I}), \quad Z_0 = \mathcal{E}(I_0)$$

$$\lambda_i^j = \max_{z \in \mathcal{Z}_{ref}} \frac{z \cdot z_i^j}{\|z\| \|z_i^j\|}, \quad 1 \leq i \leq N, 1 \leq j \leq hw$$

for $t \leftarrow T$ **to** 0 **do**

$$\epsilon \sim \mathcal{N}(0, I) \text{ if } t > 1 \text{ else } 0$$

$$\epsilon_t \sim \mathcal{N}(0, I) \text{ if } t > 1 \text{ else } 0$$

$$Z_{t-1} = \lambda(\sqrt{\alpha_{t-1}}Z + (1 - \sqrt{\alpha_{t-1}})\epsilon) +$$

$$(1 - \lambda) \left(\frac{1}{\sqrt{\alpha_t}} \left(Z_t - \frac{\beta_t}{\sqrt{1 - \alpha_t}} \epsilon_\theta(Z_t, t, c) \right) + \sigma_t \epsilon_t \right)$$

end for

$$\tilde{\mathcal{I}} = \mathcal{D}(Z_0)$$

We use these well-generated features as reference to compute the momentum coefficient λ_i^j for each latent feature $z_i^j \in Z_i$ by:

$$\lambda_i^j = \max_{z \in \mathcal{Z}_{ref}} \lambda_0 \frac{z \cdot z_i^j}{\|z\| \|z_i^j\|}, \quad (10)$$

where $\lambda_0 \geq 0$ is an adjustable coefficient to control the overall weight of momentum. Finally, we decode the denoised latent features Z_0 . We denote the overall diffusion process as Φ_λ :

$$\hat{\mathcal{I}} = \Phi_\lambda(\mathcal{I}), \quad (11)$$

where λ is the latent-level momentum coefficient in Eq. 8. The latent-level momentum is illustrated in Algorithm 1.

As shown in Figure 3, our latent-level momentum enables video diffusion models to generate a video with more details (in red boxes) and scene consistency (in blue boxes). However, such latent-level momentum limits the generation ability in unseen regions (in green boxes), where vanilla diffusion models can recover unseen regions better. Therefore, we further introduce pixel-level momentum for further enhancement of unknown areas.

Pixel-level Momentum. Previous methods that directly generate videos from input views can be considered as a

Algorithm 2 Overall Architecture

Input: Input image I_0 , camera parameters $\mathcal{K} = \{K_i\}_{i=1}^M$

Output: Gaussian parameters $\mathcal{G} = (\mu, \Sigma, \alpha, c)$

$\mathcal{G} = \text{Flash3D}(I_0)$

for $s \leftarrow 0$ to h **do**

$\mathcal{K}^s = \{K_i\}, \quad s(N-n)+1 \leq i \leq (N-n)+N$

$\mathcal{I}^s = \psi_c(\mathcal{G}, \mathcal{K}^s)$

$\mathcal{I}_{new}^s = \{I_i^{new}\} = \mu\Phi_\lambda(\mathcal{I}^s) + (1-\mu)\Phi_0(\mathcal{I}^s)$

if $s = 0$ **then**

$\mathcal{I} = \{I_0\} \cup \mathcal{I}_{new}^0$

else

$\mathcal{I} \leftarrow \mathcal{I} - \{I_i\}_{i=s(N-n)+1}^{s(N-n)+n}$

$\mathcal{I} \leftarrow \mathcal{I} \cup \mathcal{I}_{new}^s$

end if

$\mathcal{G} \leftarrow f_R(\mathcal{G}, \mathcal{I})$

end for

degenerated version ($\lambda = 0$ in Eq. 11) of our latent-level momentum:

$$\mathcal{I}_{new} = \Phi_0(\mathcal{I}), \quad (12)$$

which leads to scene inconsistency (in blue boxes). Therefore, we introduce $\Phi_\lambda(\mathcal{I})$ from Eq. 11 as pixel-level momentum to $\Phi_0(\mathcal{I})$:

$$\mathcal{I}_{new} = \mu\Phi_\lambda(\mathcal{I}) + (1-\mu)\Phi_0(\mathcal{I}), \quad (13)$$

where λ is defined as Eq. 10. Motivated by the observation that well-reconstructed areas are typically represented by Gaussians with very small volumes [19], we follow the instruction in Eq. 2 to render scale maps $\mathcal{S} = \{s_i^{j,k}\} \in [0, 1]^{N \times HW \times 3}$ by

$$s_i^{j,k} = \sum_{n \in N} (1 - S_n) \alpha_n \prod_{m=1}^{n-1} (1 - \alpha_m), \quad (14)$$

where $1 \leq i \leq N$, $1 \leq j \leq HW$ and $1 \leq k \leq 3$. Then, the pixel-level momentum coefficient $\mu = \{\mu_i^j\} \in [0, 1]^{N \times HW}$ is defined as:

$$\mu_i^j = \begin{cases} \max_k s_i^{j,k}, & \tau \leq \max_k s_i^{j,k} \\ 0, & \tau > \max_k s_i^{j,k} \end{cases} \quad (15)$$

where τ is a pre-defined threshold. Higher μ_i^j represents well-reconstructed regions, which benefits more from $\Phi_\lambda(\mathcal{I})$, while lower μ_i^j indicates unseen regions with less details, which are further enhanced by $\Phi_0(\mathcal{I})$. As shown in Figure 3e, our method can generate high-fidelity and consistent frames with cascaded momentum.

3.3. Overall Architecture

Given a single image I_0 and a sequence of camera parameters $\mathcal{K} = \{K_i\}_{i=1}^M$, our goal is to recover the underlying

scene. We first estimate the metric depth with a pre-trained network [23] and follow the instruction of Flash3D [31] by employing a encoder-decoder network to predict Gaussian parameters for each pixel. In this manner, we obtain a initial representations of the scene:

$$\mathcal{G} = \{(\mu_i, \Sigma_i, \alpha_i, c_i)\}. \quad (16)$$

Following the rendering strategy in Eq. 2, we can render a video from \mathcal{G} with camera parameters $\mathcal{K}^0 = \{K_i\}_{i=1}^N$:

$$\mathcal{I}^0 = \{I_i\}_{i=1}^N = \psi^c(\mathcal{G}, \mathcal{K}^0), \quad (17)$$

where I_i is the rendering image of the unseen viewpoint K_i . Since such rendering video \mathcal{I}^0 suffers from ambiguous geometric cues and unseen regions, we introduce a scene consistent video generation process to enhance the rendering video:

$$\mathcal{I}_{new}^0 = \mu\Phi_\lambda(\mathcal{I}^0) + (1-\mu)\Phi_0(\mathcal{I}^0). \quad (18)$$

Then, we refine the scene representations based on the input image and generated video frames $\mathcal{I} = \{I_0\} \cup \mathcal{I}^0$

$$\mathcal{G} \leftarrow f_R(\mathcal{G}, \mathcal{I}), \quad (19)$$

The target is to minimize the following 3DGS loss:

$$\mathcal{L} = \frac{1}{|\mathcal{I}|} \sum_{I \in \mathcal{I}} (1-\gamma)\mathcal{L}_1(\tilde{I}, I) + \gamma\mathcal{L}_{SSIM}(\tilde{I}, I), \quad (20)$$

where \mathcal{L}_1 , \mathcal{L}_{SSIM} denote the L_1 and SSIM loss respectively, and γ is a coefficient parameter. In this manner, we obtain enhanced Gaussian representations for the next iteration with a new sequence of camera parameters $\mathcal{K}^1 = \{K_i\}_{i=n}^{N+n}$, where n is the number of overlapped frames between two steps. Algorithm 2 describes the overall architecture of our iterative reconstruction strategy.

4. Experiments

We conduct extensive experiments to evaluate our method for 3D scene generation from single input. We first present the setup of our experiments in Section 4.1. Then, we report our qualitative and quantitative results compared to representative baseline methods in Section 4.2. We further analyze the iterative scene reconstruction process in Section 4.3. Finally, we conduct ablation studies to verify the efficacy of our framework design in Section 4.4.

4.1. Experimental setup

In our framework, we first adopt Flash3D [31] to predict Gaussian representations from the input image as initialization. The video diffusion model used for Φ_λ and Φ_0 is trained by ViewCrafter [45], with a CLIP image encoder for input image understanding. The length of videos in each

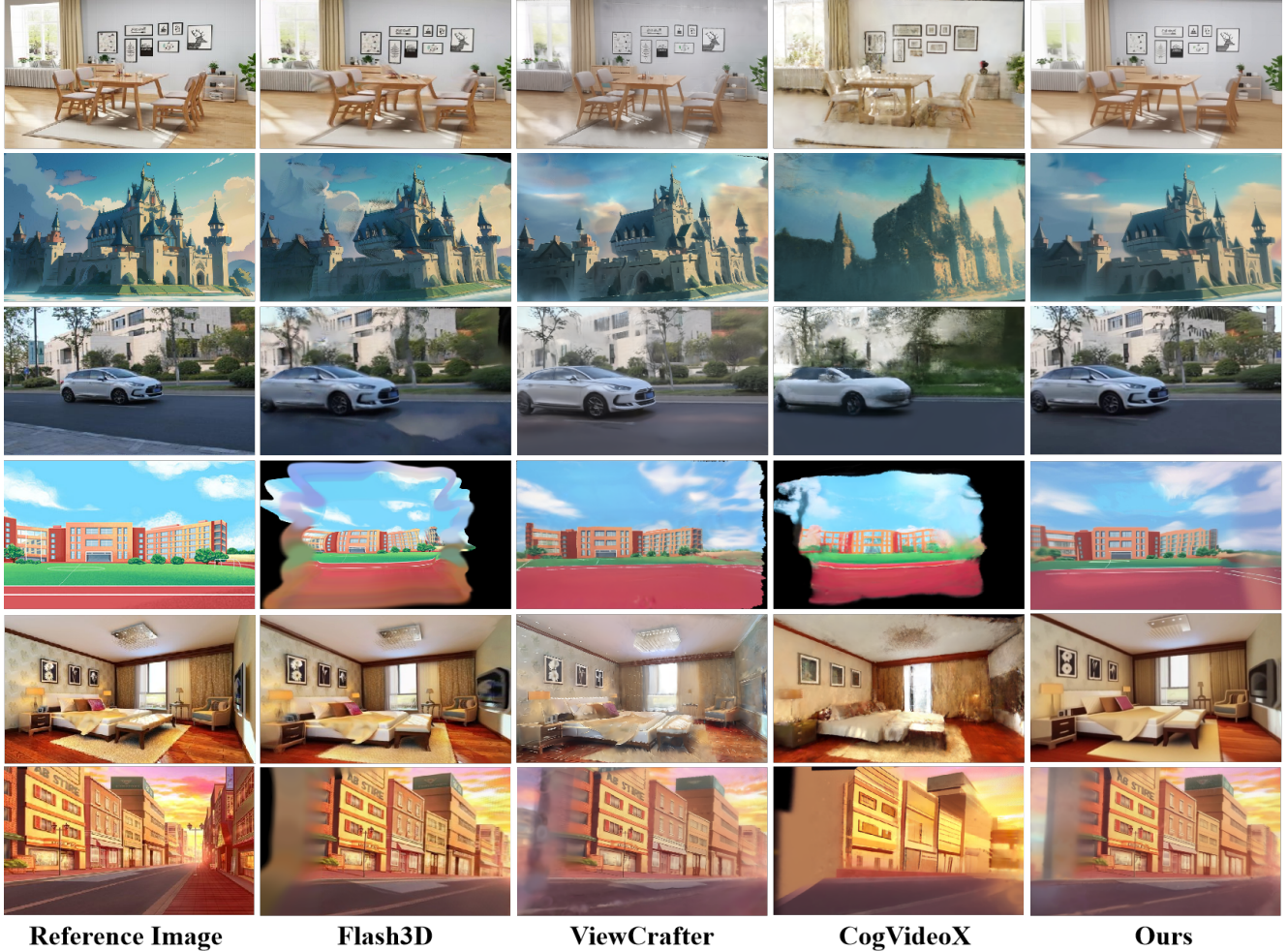


Figure 4. Qualitative comparison in 3D scene generation from single view. Given various kinds of input views, our method produces high fidelity and consistent 3D scenes.

step is set to $N = 25$ and the number of overlapped frames between two steps is set to $n = 10$. The number of total iterations h is adapted to the length of camera trajectory. In each iteration, we optimize Gaussian representations for 5000 steps with $\gamma = 0.2$. The densification interval is set to 100, and the opacity of Gaussians is reset every 3000 steps.

For 3D scene generation from single image, we compare our methods with one regression-based method [31] and two generative-based methods [42, 45]. Specifically, Flash3D [31] uses a frozen off-the-shelf network [23] for depth estimation to predict the first layer of Gaussians and adds additional layers of Gaussians that are offset in space. The model is pre-trained on the RealEstate10k [48] dataset. CogVideoX [42] is a large-scale video generation model based on diffusion transformer, trained on 35M video clips and 2B images. We adopt the most powerful version of CogVideoX [42], which has 5B parameters. ViewCrafter [45] introduces a point-conditioned video diffusion and iterative camera trajectory. For quantitative re-

sults, We construct a subset of RealEstate10K [48] for evaluation. The easy test set has smaller movement of view-points, and the hard set has larger view ranges. We employ PSNR, SSIM [37] and LPIPS [46] as the evaluation metrics for rendering image quality.

4.2. 3D Scene Generation

Qualitative Results. As shown in Figure 4, we visualize the final rendering results of our method and baselines. Unambiguous geometric cues are unavailable for Flash3D [31] from single input, leading to distortions of the table and chairs in row 1, column 2. Besides, it also lack the ability to recover unseen regions, which is obvious in the zoom-out setting, as shown in row 4, column 2. ViewCrafter [45] and CogVideoX [42] can enhance the input frames, but suffer from scene inconsistency, which leads to conflicts in further reconstruction. For example, CogVideoX [42] generates different chairs compared to the input image in row 1, and ViewCrafter [45] changes the color style of the scene in

Table 1. Quantitative comparison in 3D scene generation from single view. We report the average results of PSNR, SSIM and LPIPS. Our approach outperforms other baselines in all metrics.

Method	Easy Set			Hard Set		
	PSNR \uparrow	SSIM \uparrow	LPIPS \downarrow	PSNR \uparrow	SSIM \uparrow	LPIPS \downarrow
Flash3D [31]	17.94	0.682	0.160	14.41	0.599	0.370
CogVideoX [42]	17.25	0.710	0.352	15.42	0.636	0.415
ViewCrafter [45]	20.70	0.794	0.159	15.63	0.676	0.258
Ours	20.95	0.800	0.145	17.62	0.707	0.233



Figure 5. Visualization of rendering results in each iteration. The inconsistency in CogVideoX [42] and ViewCrafter [45] gradually increases. Our method can maintain high consistency during the iterative reconstruction process.

row 3. Our cascaded momentum can provide high quality observations while maintaining the scene consistency. The various styles of inputs, from cartoon to realistic images, from indoor to outdoor scenes, also demonstrate the generalization ability of our method.

Quantitative Results. The quantitative comparison results are reported in Table 1. For the easy test set, the simple employment of CogVideoX [42] leads to worse performance in PSNR and LPIPS, which demonstrates the negative effects of inconsistent generation. With the same video diffusion model, our method outperforms ViewCrafter [45] in all metrics on the easy set, and shows greater advantages on the hard set. The lower LPIPS score further demonstrates that our approach generates more perceptually accurate images.

4.3. Iterative Gaussian Reconstruction

Our paradigm follows an iterative Gaussian reconstruction process to avoid the restriction of video length in video diffusion models. Under this circumstance, the inconsistency of generated videos will be accumulated in each iteration. As shown in Figure 5, although ViewCrafter [45] and CogVideoX [42] maintain decent performance in the first two iterations, they fail to reconstruct a reasonable scene in further iterations with larger view ranges. Benefiting from cascaded momentum, our method maintains scene consistency

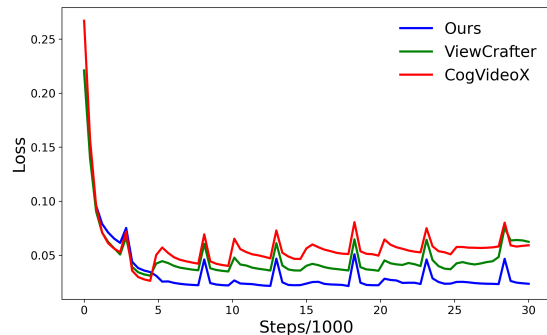


Figure 6. Reconstruction loss in optimization of Gaussian representations. The overall process includes 5 iterations, where we optimize 3DGS for 5000 steps in each iteration.

during iterative reconstruction for the global Gaussian representations. We also visualize the 3DGS loss in Figure 6. The reconstruction process in CogVideoX [42] and ViewCrafter [45] can not fully converge due to the inconsistency between different frames. At the end of reconstruction, their losses are even higher than those at the end of the first step. In contrast, our method can converge to a lower loss value at each iteration with more consistent novel views as supervision information of Gaussian optimization.



Figure 7. Visualization of the ablation study.

4.4. Ablation Study

We conduct ablation studies to investigate our momentum-based 3D generation paradigm. We report the quantitative results in Table 2 and visualize the rendering results in Figure 7. Without any generative prior knowledge, our framework degenerates to Flash3D [31], where rendering results in column 5 suffer from distortions in geometry, since the estimation of depth is not fully supervised in monocular settings. This issue leads to a decrease of 3.67dB in PSNR and 0.126 in SSIM. The third column in Figure 7 illustrates that the absence of latent-level momentum results in the change of existing components. Such experimental results demonstrate the ability of latent-level momentum to preserve scene consistency. We also remove the pixel-level momentum in our paradigm. Lack of pixel-level momentum restricts the generation ability of diffusion models, with a decrease of 3.5dB in PSNR and 0.111 in SSIM.

5. Conclusion and Discussion

In this paper, we propose a momentum-based paradigm to generate 3D scene from single image. We generate noisy samples from the original features to serve as momentum, thereby enhancing video details and preserving scene consistency. Nevertheless, when it comes to latent features with a perception field that spans both known and unknown regions, the latent-level momentum can impede the generative capacity within the unknown areas. To overcome this limitation, we incorporate the previously mentioned consistent video as a pixel-level momentum to a video generated directly without momentum, aiming to achieve a more effective recovery of unseen regions. This cascaded momentum strategy empowers video diffusion models to produce both high-fidelity and consistent novel views. We further re-

fine the global Gaussian representations using the enhanced frames and render new frames for the momentum update in the subsequent step. This iterative process allows us to reconstruct a 3D scene, bypassing the constraints typically associated with video length. Comprehensive experiments have demonstrated the generalization capability and the superior performance of our method in generating scenes that are both high-fidelity and consistent.

Table 2. Ablation study of our Scene Splatter. We report the average PSNR, SSIM and LPIPS of rendering results.

Methods	PSNR	SSIM	LPIPS
Ours	19.81	0.770	0.169
w.o. video diffusion model	16.14	0.644	0.268
w.o. latent-level momentum	18.52	0.748	0.194
w.o. pixel-level momentum	16.31	0.659	0.278

Limitations and Future Works. Although our method can generate high fidelity and consistent 3D scene from one single image, the employment of video diffusion models requires longer time compared to regression-based models (e.g. Flash3D [31]). The iterative strategy further exacerbates the consumption of time. Besides, our method is now restricted to static 3D scene generation, where our 3D representations lack the ability to recover 4D scenes. In the future, we will focus on the efficiency of 3D scene generation models to further compress the time consumption. We are also interested in generating 4D scenes by decoupling the temporal and spatial factors in video diffusion.

Acknowledgments This work was supported in part by the National Natural Science Foundation of China under Grant 62206147, and in part by 2024 WeChat Vision, Tencent Inc. Rhino-Bird Focused Research Program.

References

- [1] Andreas Blattmann, Tim Dockhorn, Sumith Kulal, Daniel Mendelevitch, Maciej Kilian, Dominik Lorenz, Yam Levi, Zion English, Vikram Voleti, Adam Letts, et al. Stable video diffusion: Scaling latent video diffusion models to large datasets. *arXiv preprint arXiv:2311.15127*, 2023. 3, 4
- [2] David Charatan, Sizhe Lester Li, Andrea Tagliasacchi, and Vincent Sitzmann. pixelsplat: 3d gaussian splats from image pairs for scalable generalizable 3d reconstruction. In *CVPR*, pages 19457–19467, 2024. 2
- [3] Anpei Chen, Zexiang Xu, Fuqiang Zhao, Xiaoshuai Zhang, Fanbo Xiang, Jingyi Yu, and Hao Su. Mvsnerf: Fast generalizable radiance field reconstruction from multi-view stereo. In *ICCV*, pages 14124–14133, 2021. 2
- [4] Haoxin Chen, Yong Zhang, Xiaodong Cun, Menghan Xia, Xintao Wang, Chao Weng, and Ying Shan. Videocrafter2: Overcoming data limitations for high-quality video diffusion models, 2024. 3
- [5] Yuedong Chen, Haofei Xu, Chuanxia Zheng, Bohan Zhuang, Marc Pollefeys, Andreas Geiger, Tat-Jen Cham, and Jianfei Cai. Mvsplat: Efficient 3d gaussian splatting from sparse multi-view images. In *ECCV*, pages 370–386. Springer, 2024. 2
- [6] Zilong Chen, Yikai Wang, Feng Wang, Zhengyi Wang, and Huaping Liu. V3d: Video diffusion models are effective 3d generators. *arXiv preprint arXiv:2403.06738*, 2024. 3
- [7] Julian Chibane, Aayush Bansal, Verica Lazova, and Gerard Pons-Moll. Stereo radiance fields (srf): Learning view synthesis for sparse views of novel scenes. In *CVPR*, pages 7911–7920, 2021. 2
- [8] Rafail Fridman, Amit Abecasis, Yoni Kasten, and Tali Dekel. Scenescape: Text-driven consistent scene generation. *NeurIPS*, 36, 2023. 2
- [9] Hao He, Yinghao Xu, Yuwei Guo, Gordon Wetzstein, Bo Dai, Hongsheng Li, and Ceyuan Yang. Cameractrl: Enabling camera control for text-to-video generation. *arXiv preprint arXiv:2404.02101*, 2024. 2, 3
- [10] Yingqing He, Tianyu Yang, Yong Zhang, Ying Shan, and Qifeng Chen. Latent video diffusion models for high-fidelity long video generation. *arXiv*, 2022. 3
- [11] Jonathan Ho, Ajay Jain, and Pieter Abbeel. Denoising diffusion probabilistic models. *NeurIPS*, 33:6840–6851, 2020. 2
- [12] Bernhard Kerbl, Georgios Kopanas, Thomas Leimkühler, and George Drettakis. 3d gaussian splatting for real-time radiance field rendering. *ACM Trans. Graph.*, 42(4):139–1, 2023. 2, 3
- [13] Yao-Chih Lee, Yi-Ting Chen, Andrew Wang, Ting-Hsuan Liao, Brandon Y Feng, and Jia-Bin Huang. Vividdream: Generating 3d scene with ambient dynamics. *arXiv preprint arXiv:2405.20334*, 2024. 2
- [14] Jiahao Li, Hao Tan, Kai Zhang, Zexiang Xu, Fujun Luan, Yinghao Xu, Yicong Hong, Kalyan Sunkavalli, Greg Shakhnarovich, and Sai Bi. Instant3d: Fast text-to-3d with sparse-view generation and large reconstruction model. *arXiv preprint arXiv:2311.06214*, 2023. 2
- [15] Weiyu Li, Rui Chen, Xuelin Chen, and Ping Tan. Sweet-dreamer: Aligning geometric priors in 2d diffusion for consistent text-to-3d. *arXiv preprint arXiv:2310.02596*, 2023. 2
- [16] Chen-Hsuan Lin, Jun Gao, Luming Tang, Towaki Takikawa, Xiaohui Zeng, Xun Huang, Karsten Kreis, Sanja Fidler, Ming-Yu Liu, and Tsung-Yi Lin. Magic3d: High-resolution text-to-3d content creation. In *CVPR*, pages 300–309, 2023. 2
- [17] Minghua Liu, Chao Xu, Haian Jin, Linghao Chen, Mukund Varma T, Zexiang Xu, and Hao Su. One-2-3-45: Any single image to 3d mesh in 45 seconds without per-shape optimization. *NeurIPS*, 36, 2023. 2
- [18] Ruoshi Liu, Rundi Wu, Basile Van Hoorick, Pavel Tokmakov, Sergey Zakharov, and Carl Vondrick. Zero-1-to-3: Zero-shot one image to 3d object. In *ICCV*, pages 9298–9309, 2023. 2
- [19] Xi Liu, Chaoyi Zhou, and Siyu Huang. 3dgs-enhancer: Enhancing unbounded 3d gaussian splatting with view-consistent 2d diffusion priors. *NeurIPS*, 2024. 2, 5
- [20] Xiaoxiao Long, Yuan-Chen Guo, Cheng Lin, Yuan Liu, Zhiyang Dou, Lingjie Liu, Yuexin Ma, Song-Hai Zhang, Marc Habermann, Christian Theobalt, et al. Wonder3d: Single image to 3d using cross-domain diffusion. In *CVPR*, pages 9970–9980, 2024. 2
- [21] Andreas Lugmayr, Martin Danelljan, Andres Romero, Fisher Yu, Radu Timofte, and Luc Van Gool. Repaint: Inpainting using denoising diffusion probabilistic models. In *CVPR*, pages 11461–11471, 2022. 4
- [22] Ben Mildenhall, Pratul P Srinivasan, Matthew Tancik, Jonathan T Barron, Ravi Ramamoorthi, and Ren Ng. Nerf: Representing scenes as neural radiance fields for view synthesis. *Communications of the ACM*, 65(1):99–106, 2021. 2
- [23] Luigi Piccinelli, Yung-Hsu Yang, Christos Sakaridis, Mattia Segu, Siyuan Li, Luc Van Gool, and Fisher Yu. Unidepth: Universal monocular metric depth estimation. In *CVPR*, pages 10106–10116, 2024. 5, 6
- [24] Aditya Ramesh, Prafulla Dhariwal, Alex Nichol, Casey Chu, and Mark Chen. Hierarchical text-conditional image generation with clip latents. *arXiv preprint arXiv:2204.06125*, 1(2):3, 2022. 2
- [25] Konstantinos Rematas, Ricardo Martin-Brualla, and Vittorio Ferrari. Sharf: Shape-conditioned radiance fields from a single view. *CVPR*, 2021. 2
- [26] Robin Rombach, Andreas Blattmann, Dominik Lorenz, Patrick Esser, and Björn Ommer. High-resolution image synthesis with latent diffusion models. In *CVPR*, pages 10684–10695, 2022. 2, 4
- [27] Chitwan Saharia, William Chan, Saurabh Saxena, Lala Li, Jay Whang, Emily L Denton, Kamyar Ghasemipour, Raphael Gontijo Lopes, Burcu Karagol Ayan, Tim Salimans, et al. Photorealistic text-to-image diffusion models with deep language understanding. *NeurIPS*, 35:36479–36494, 2022. 2
- [28] Yichun Shi, Peng Wang, Jianglong Ye, Mai Long, Kejie Li, and Xiao Yang. Mvdream: Multi-view diffusion for 3d generation. *arXiv preprint arXiv:2308.16512*, 2023. 2

- [29] Jaidev Shriram, Alex Trevithick, Lingjie Liu, and Ravi Ramamoorthi. Realdreamer: Text-driven 3d scene generation with inpainting and depth diffusion. *arXiv preprint arXiv:2404.07199*, 2024. [2](#), [3](#)
- [30] Jiaming Song, Chenlin Meng, and Stefano Ermon. Denoising diffusion implicit models. *ICLR*, 2021. [2](#)
- [31] Stanislaw Szymanowicz, Eldar Insafutdinov, Chuanxia Zheng, Dylan Campbell, João F Henriques, Christian Rupprecht, and Andrea Vedaldi. Flash3d: Feed-forward generalisable 3d scene reconstruction from a single image. *NeurIPS*, 2024. [1](#), [2](#), [3](#), [4](#), [5](#), [6](#), [7](#), [8](#)
- [32] Stanislaw Szymanowicz, Christian Rupprecht, and Andrea Vedaldi. Splatter image: Ultra-fast single-view 3d reconstruction. In *CVPR*, pages 10208–10217, 2024. [2](#)
- [33] Jiayang Tang, Zhaoxi Chen, Xiaokang Chen, Tengfei Wang, Gang Zeng, and Ziwei Liu. Lgm: Large multi-view gaussian model for high-resolution 3d content creation. In *ECCV*, pages 1–18. Springer, 2024. [2](#)
- [34] Alex Trevithick and Bo Yang. Grf: Learning a general radiance field for 3d representation and rendering. In *ICCV*, pages 15182–15192, 2021. [2](#)
- [35] Vikram Voleti, Chun-Han Yao, Mark Boss, Adam Letts, David Pankratz, Dmitry Tochilkin, Christian Laforte, Robin Rombach, and Varun Jampani. Sv3d: Novel multi-view synthesis and 3d generation from a single image using latent video diffusion. In *ECCV*, pages 439–457. Springer, 2024. [3](#)
- [36] Yunsong Wang, Tianxin Huang, Hanlin Chen, and Gim Hee Lee. Freesplat: Generalizable 3d gaussian splatting towards free-view synthesis of indoor scenes. *NeurIPS*, 2024. [2](#)
- [37] Zhou Wang, Alan C Bovik, Hamid R Sheikh, and Eero P Simoncelli. Image quality assessment: from error visibility to structural similarity. *TIP*, 13(4):600–612, 2004. [6](#)
- [38] Zhengyi Wang, Cheng Lu, Yikai Wang, Fan Bao, Chongxuan Li, Hang Su, and Jun Zhu. Prolificdreamer: High-fidelity and diverse text-to-3d generation with variational score distillation. *NeurIPS*, 36, 2024. [2](#)
- [39] Zhouxia Wang, Ziyang Yuan, Xintao Wang, Yaowei Li, Tianshui Chen, Menghan Xia, Ping Luo, and Ying Shan. Motionctrl: A unified and flexible motion controller for video generation. In *SIGGRAPH*, pages 1–11, 2024. [2](#), [3](#)
- [40] Rundi Wu, Ben Mildenhall, Philipp Henzler, Keunhong Park, Ruiqi Gao, Daniel Watson, Pratul P Srinivasan, Dor Verbin, Jonathan T Barron, Ben Poole, et al. Reconfusion: 3d reconstruction with diffusion priors. In *CVPR*, pages 21551–21561, 2024. [2](#)
- [41] Jinbo Xing, Menghan Xia, Yong Zhang, Haoxin Chen, Wangbo Yu, Hanyuan Liu, Gongye Liu, Xintao Wang, Ying Shan, and Tien-Tsin Wong. Dynamicrafter: Animating open-domain images with video diffusion priors. In *ECCV*, pages 399–417. Springer, 2024. [3](#), [4](#)
- [42] Zhuoyi Yang, Jiayan Teng, Wendi Zheng, Ming Ding, Shiyu Huang, Jiazheng Xu, Yuanming Yang, Wenyi Hong, Xiaohan Zhang, Guanyu Feng, et al. Cogvideox: Text-to-video diffusion models with an expert transformer. *arXiv preprint arXiv:2408.06072*, 2024. [1](#), [2](#), [3](#), [4](#), [6](#), [7](#)
- [43] Alex Yu, Vickie Ye, Matthew Tancik, and Angjoo Kanazawa. pixelnerf: Neural radiance fields from one or few images. In *CVPR*, pages 4578–4587, 2021. [2](#)
- [44] Hong-Xing Yu, Haoyi Duan, Junhwa Hur, Kyle Sargent, Michael Rubinstein, William T Freeman, Forrester Cole, Deqing Sun, Noah Snavely, Jiajun Wu, et al. Wonderjourney: Going from anywhere to everywhere. In *CVPR*, pages 6658–6667, 2024. [3](#)
- [45] Wangbo Yu, Jinbo Xing, Li Yuan, Wenbo Hu, Xiaoyu Li, Zhipeng Huang, Xiangjun Gao, Tien-Tsin Wong, Ying Shan, and Yonghong Tian. Viewcrafter: Taming video diffusion models for high-fidelity novel view synthesis. *arXiv preprint arXiv:2409.02048*, 2024. [1](#), [2](#), [3](#), [4](#), [5](#), [6](#), [7](#)
- [46] Richard Zhang, Phillip Isola, Alexei A Efros, Eli Shechtman, and Oliver Wang. The unreasonable effectiveness of deep features as a perceptual metric. In *CVPR*, pages 586–595, 2018. [6](#)
- [47] Shengjun Zhang, Xin Fei, Fangfu Liu, Haixu Song, and Yueqi Duan. Gaussian graph network: Learning efficient and generalizable gaussian representations from multi-view images. *NeurIPS*, 37:50361–50380, 2024. [2](#)
- [48] Tinghui Zhou, Richard Tucker, John Flynn, Graham Fyffe, and Noah Snavely. Stereo magnification: Learning view synthesis using multiplane images. *arXiv preprint arXiv:1805.09817*, 2018. [6](#)